Materials Letters 172 (2016) 102–104

Contents lists available at ScienceDirect

Materials Letters

journal homepage: www.elsevier.com/locate/matlet

Variations of phase constitution and magnetic properties with Ce content in Ce-Fe-B permanent magnets

Zhu-bai Li [a,b], Ming Zhang [b], Bao-gen Shen [b,*], Feng-xia Hu [b], Ji-rong Sun [b]

[a] Key Laboratory of Integrated Exploitation of Bayan Obo Multi-Metal Resources, Inner Mongolia University of Science and Technology, Baotou 014010, China
[b] State Key Laboratory for Magnetism, Institute of Physics, Chinese Academy of Sciences, Beijing 100190, China

ARTICLE INFO

Article history:
Received 4 November 2015
Received in revised form
23 February 2016
Accepted 27 February 2016
Available online 2 March 2016

Keywords:
Magnetic materials
$Ce_2Fe_{14}B$
X-ray techniques
Magnetic properties

ABSTRACT

Magnetic materials of $Ce_{12+x}Fe_{82-x}B_6$ (x=0, 0.5, 1, 1.5, 2, and 3) containing mainly $Ce_2Fe_{14}B$ phase were prepared by melt spinning method. The coercivity is the lowest in $Ce_{12}Fe_{81}B_6$ ribbons. With the increase of Ce content, the coercivity increases monotonically, and X-ray techniques show that the amount of minor phase Fe_3B decreases but the amount of $CeFe_2$ increases. Magnetization reversal and magnetic properties are dependent on the amount of minor phases. The squareness of hysteresis loop is the best in $Ce_{13.5}Fe_{80.5}B_6$ ribbons with energy product of 6.80 MGOe. Optimizing the phase constitution is necessary to improve magnetic properties in Ce-based alloys for utilizing the rare earth resource in a balanced manner.

1. Introduction

Rare earth permanent magnets $Re_2Fe_{14}B$ (R=Nd, Pr) are widely used in many fields ranging from computers, miniature speakers, automotive industry to wind generators due to their high coercivity and energy product [1–3]. But the wide application and mass production of $(NdPr)_2Fe_{14}B$ brings a series of problems both on the resource and on the environment in the mining and extraction processes of rare earth elements. Since the rare earth mineral is paragenetic ore, the over-consumption of less abundant rare earth Nd and Pr causes the overstock of the most abundant rare earth La and Ce [4,5]. Theoretically, $Ce_2Fe_{14}B$ magnets, bearing anisotropy field of 26 kOe [6], is potential candidate with moderate performance plugging the gap between those of ferrite and $(NdPr)_2Fe_{14}B$ [7]. Developing high abundant rare earth magnets is urgent not only for reducing the cost but for protecting natural resources [8–12].

Actually, the magnetic properties of $Ce_2Fe_{14}B$ prepared in laboratory are much inferior to those of $Nd_2Fe_{14}B$ magnets [13,14], and there is something difference in phase diagram and phase constitution between Ce-Fe-B and Nd-Fe-B alloys [13,15]. Since magnetic properties are sensitive to the microstructure, a little difference in phase constitution possibly results in a large variation in coercivity. For better understanding the feature in Ce-Fe-B alloys, in this letter we prepared Ce-Fe-B ribbons via melt spinning method, and the variation of phase constitution with Ce content is systematically investigated combined with the analysis of magnetic properties, which is expected to serve as a reference for preparing high abundant rare earth magnets.

2. Experiment

The precursor ingots $Ce_{12+x}Fe_{82-x}B_6$ (x=0, 0.5, 1, 1.5, 2 and 3) were produced by arc-melting constituent metals with purity better than 99.9 wt% under an argon atmosphere. In order to make the ingots homogeneous in chemical composition, they are turned over and melted at least three times. The ribbons were obtained by induction melting the ingot and then ejected the melt by pressurized argon onto the surface of a rotating copper wheel. For optimizing magnetic properties the wheel surface was polished using the 1000-grit paper. The phase constitution and grain size were examined by x-ray diffraction (XRD) using Cu Kα radiation. Magnetic measurements were performed with Lakeshore vibrating sample magnetometer (VSM).

3. Results and discussion

Melt-spinning is a rapid quenching method to prepare ribbons with nanocrystalline structure. Fig. 1 shows XRD patterns for $Ce_{12}Fe_{82}B_6$, $Ce_{13.5}Fe_{80.5}B_6$ and $Ce_{15}Fe_{79}B_6$ melt-spun ribbons. According to the intensities of diffraction peak all samples contain

* Corresponding author.
E-mail address: shenbg@iphy.ac.cn (B.-g. Shen).

http://dx.doi.org/10.1016/j.matlet.2016.02.149
0167-577X/

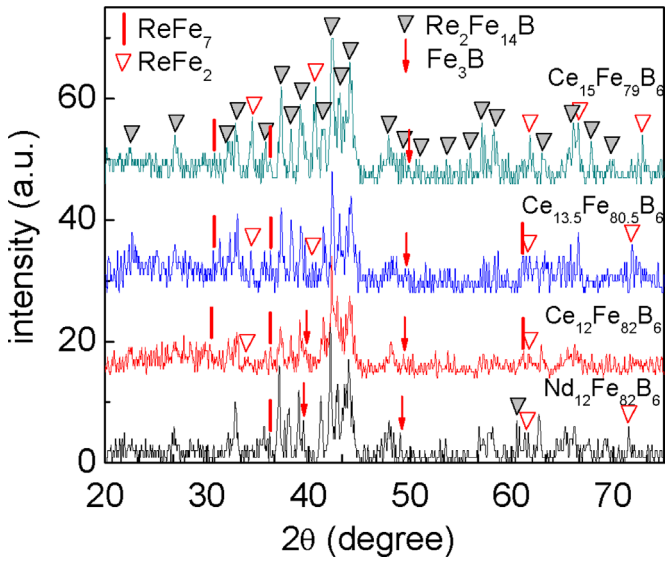

Fig. 1. XRD patterns for $Ce_{12}Fe_{82}B_6$, $Ce_{13.5}Fe_{80.5}B_6$, $Ce_{15}Fe_{79}B_6$ and $Nd_{12}Fe_{82}B_6$ ribbons.

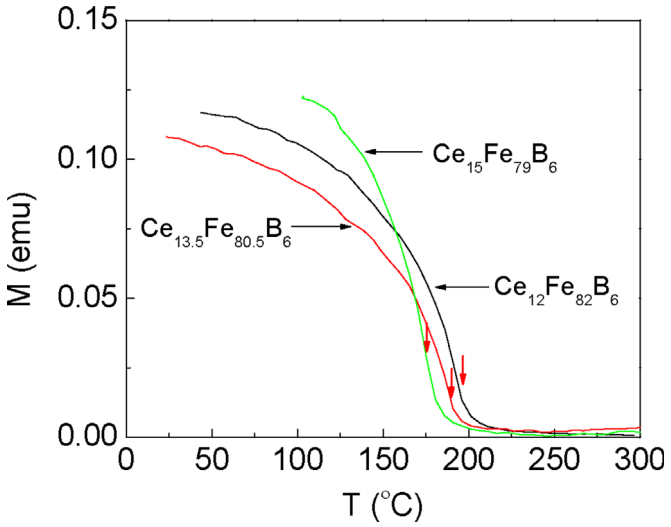

Fig. 2. The variations of magnetization with temperature under the field of 1 kOe for $Ce_{12}Fe_{82}B_6$, $Ce_{13.5}Fe_{80.5}B_6$ and $Ce_{15}Fe_{79}B_6$ ribbons.

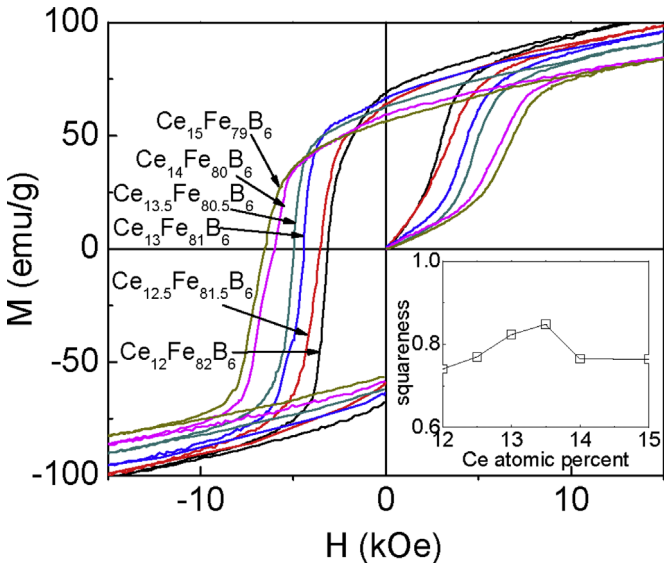

Fig. 3. The hysteresis loops for Ce-Fe-B ribbons at room temperature. The inset shows the dependence of squareness on the Ce atomic percent.

the main phase of $Ce_2Fe_{14}B$, but the diffraction peaks are not very smooth and there are some weak peaks, indicating a little amount of amorphous phase and minor phases existing in these ribbons. Using Jade software the average grain sizes are estimated to be in the range of 20–30 nm. For a comparison, the XRD pattern of $Nd_{12}Fe_{82}B_6$ ribbons is also shown in Fig. 1. It can be seen that $Nd_{12}Fe_{82}B_6$ contains the minor phases of Fe_3B, $ReFe_2$, and $ReFe_7$. For counterpart $Ce_{12}Fe_{82}B_6$ for optimizing the squareness of hysteresis loop the wheel velocity was 27 m/s in melt-spinning, larger than 23–25 m/s for other samples. The intensities of diffraction peak are a little lower in $Ce_{12}Fe_{82}B_6$ ribbons, indicating that the average grain size is smaller and that there is more amount of amorphous phase in the ribbons, but the diffraction peaks of $ReFe_7$ and $ReFe_2$ are also evident. Ce-Fe-B alloys has a different phase diagram from that of Nd-Fe-B [13,15]. The residual Fe and $CeFe_2$ also coexist with $Ce_2Fe_{14}B$ phase using strip-casting method [15,16]. It seems difficult to suppress the formation of minor phases in preparing Ce-Fe-B ribbons by rapid solidification. According to the variation of peak intensities, combined with Rietveld analysis using the Rietica software the amount of Fe_3B decreases with the increase of Ce content, but the amount of $CeFe_2$ phase increases. In $Ce_{15}Fe_{79}B_6$ ribbons the amounts of Fe_3B and $CeFe_2$ are 3 wt% and 13 wt%, respectively. Neglecting the amount of amorphous phase, the mass percents of main phase $Re_2Fe_{14}B$ are 89%, 87%, 90%, and 83%, receptively, for $Nd_{12}Fe_{82}B_6$, $Ce_{12}Fe_{82}B_6$, $Ce_{13.5}Fe_{80.5}B_6$, and $Ce_{15}Fe_{79}B_6$ ribbons.

In order to check the effect of phase constitution, Curie temperature was measured for $Ce_{12}Fe_{82}B_6$, $Ce_{13.5}Fe_{80.5}B_6$ and $Ce_{15}Fe_{79}B_6$, respectively. Firstly, magnetized the sample to saturation, and then increased temperature and recorded the magnetization under a magnetic field of 1 kOe (shown in Fig. 2). Even with the different phase constitution, the Curie temperatures, which are shown by the arrows, don't show a large variation among these three samples. The slight difference in Curie temperature may lie in the defects in $Ce_2Fe_{14}B$ phase. The high Ce content and low Fe content in Ce-Fe-B alloys leads possibly to increase the vacancies in the Fe sublattices, which may decrease a little the Curie temperature.

Curie temperature is the intrinsic properties determined mainly by the main phase, but coercivity and remanence are sensitive to the microstructure and phase constitution. Fig. 3 shows the hysteresis loops for Ce-Fe-B ribbons, and the magnetic properties, i.e., coercivity, remanence, and energy product are listed in Table 1. In $Ce_{12}Fe_{82}B_6$ the coercivity is the lowest with low remanence and energy product, which is partially due to the larger amount of minor phases. With the increase of Ce content, the coercivity increases monotonically, but both the remanence and energy product are abnormal dependent on the Ce atomic percent. As Ce atomic percent increases to 13.5 the amount of minor phases reduces, and the coercivity reaches to 4.96 kOe with energy product of 6.80 MGOe. With the continuing increase of Ce atomic

Table 1
Magnetic properties for Ce-Fe-B ribbons at room temperature.

Composition	H_c (kOe)	M_r (emu/g)	Squareness	$(BH)_{max}$ (MGOe)
$Ce_{12}Fe_{82}B_6$	3.11	68.93	0.74	5.57
$Ce_{12.5}Fe_{81.5}B_6$	3.54	63.98	0.77	5.75
$Ce_{13}Fe_{81}B_6$	4.43	66.84	0.82	7.31
$Ce_{13.5}Fe_{80.5}B_6$	4.96	63.01	0.85	6.80
$Ce_{14}Fe_{80}B_6$	6.01	59.41	0.77	5.82
$Ce_{15}Fe_{79}B_6$	6.54	56.25	0.76	5.70

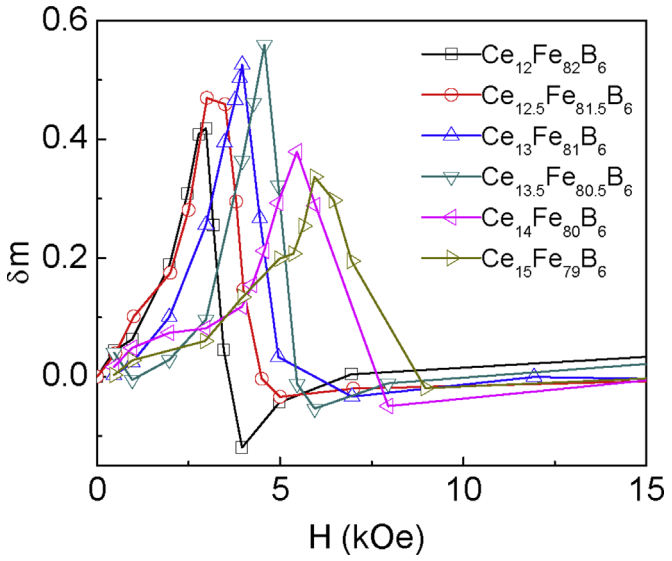

Fig. 4. δm curves (Henkel plots) for Ce-Fe-B ribbons.

percent, both the remanence and energy product decrease due to a growing increase in the amount of $CeFe_2$ phase.

The uniform magnetization reversals and better squareness of hysteresis loop are necessary for obtaining high magnetic properties. For well exchange-coupled isotropic magnets with nanostructure, the amount of intergranular soft phase has an effect on the magnetization reversal [17]. The squareness of hysteresis loop in second quadrant, which determined by the ratio of the integral $\int_0^{-H_c} M/M_s dH$ to $M_r/M_s{*}H_c$ (the product of remanence and coercivity), can reflect the uniformity of magnetization reversal [17]. As shown in the inset of Fig. 3, the squareness of hysteresis loop is improved with the increase of Ce atomic percent, peaks for the 13.5 at%, and then declines. Since the demagnetization curves do not show a two-step reversal characteristic among these samples, the more uniform magnetization reversal in $Ce_{13.5}Fe_{80.5}B_6$ ribbons should be mainly attributed to the least amount of contained minor phases [17].

Henkel plots, defined as $\delta m = [2M_r(H) + M_d(H)]/M_r - 1$, are also used to evaluate the intergranular exchange coupling effect [17]. Here $M_r(H)$ and $M_d(H)$ are the initial remanence and demagnetization remanence, respectively, and M_r is the saturation remanence. Positive value of δm implies the existing of intergranular exchange coupling. As shown in Fig. 4, the variation of δm maximum value with the Ce content is consistent with that of squareness in these Ce-Fe-B ribbons. In *Pr*-Fe-B ribbons, δm value peaks a maximum of 0.91 for Pr atomic percent 12.6% in $Pr_{12.6}Fe_{81.4}B_6$ ribbons [18], and for $Nd_{12}Fe_{82}B_6$ ribbons the maximum of δm value reaches to 1.14 [17]. But in Ce-Fe-B ribbons it is for Ce atomic percent 13.5% that δm value reaches a maximum of 0.56. δm value is also dependent on the amount of intergranular phase in the well exchange-coupled magnets [17]. So the variation of δm value and the low maximum of δm value also show the difference of phase constitution between Ce-Fe-B and Nd(Pr)-Fe-B alloys.

4. Conclusions

In summary, there exist minor phases, i.e., Fe_3B, $CeFe_7$ $CeFe_2$ and amorphous phase in Ce-Fe-B ribbons. With the increase of Ce content, accompanied by an increase of coercivity, the amount of Fe_3B phase decreases but the amount of $CeFe_2$ phase increases. The squareness of hysteresis loop and δm value demonstrate that the phase constitution of Ce-Fe-B is different from that of Nd(Pr)-Fe-B alloys, and optimizing the composition designing and phase constitution is necessary to improve magnetic properties in Ce-based permanent magnets.

Acknowledgements

The present work was supported by the National Basic Research Program of China (Grant no. 2014CB643702) and the National Natural Science Foundation of China (Grant no. 51461033).

References

[1] M. Sagawa, J. Mater. Eng. Perform. 22 (2013) 2860–2866.
[2] J.J. Croat, J.F. Herbst, R.W. Lee, F.E. Pinkerton, Appl. Phys. Lett. 44 (1984) 148–149.
[3] J.J. Ni, T.Y. Ma, M. Yan, Mater. Lett. 75 (2012) 1–3.
[4] M.G. Zhu, W. Li, J.D. Wang, L.Y. Zheng, Y.F. Li, K. Zhang, H.B. Feng, T. Liu, IEEE Trans. Magn. 50 (2014) 1000104.
[5] M. Zhang, Z.B. Li, B.G. Shen, F.X. Hu, J.R. Sun, J. Alloy. Compd. 651 (2015) 144–148.
[6] J.F. Herbst, Rev. Mod. Phys. 63 (1991) 819–898.
[7] J.M.D. Coey, Scr. Mater. 67 (2012) 524–529.
[8] S.L. Huang, H.B. Feng, M.G. Zhu, A.H. Li, Y. Zhang, W. Li, AIP Adv. 4 (2014) 107127.
[9] A.K. Pathak, M. Khan, K.A. Gschneidner Jr, R.W. McCallum, L. Zhou, K.W. Sun, K. W. Dennis, C. Zhou, F.E. Pinkerton, M.J. Kramer, V.K. Pecharsky, Adv. Mater. 27 (2015) 2663–2667.
[10] Z.B. Li, B.G. Shen, M. Zhang, F.X. Hu, J.R. Sun, J. Alloy. Compd. 628 (2015) 325–328.
[11] W. Gong, G.C. Hadjipanayis, J. Appl. Phys. 63 (1988) 3513–3515.
[12] L.H. Chu, Y. Liu, J. Li, Y.L. Ma, C.Y. Li, IEEE Trans. Magn. 48 (2012) 2092–2095.
[13] J.F. Herbst, M.S. Meyer, F.E. Pinkerton, J. Appl. Phys. 111 (2012) 07A718.
[14] M.Y. Xing, J.Z. Han, Z. Lin, F.M. Wan, C. Li, S.Q. Liu, C.S. Wang, J.B. Yang, Y. C. Yang, J. Magn. Magn. Mater. 331 (2013) 140–143.
[15] C.J. Yan, S. Guo, R.J. Chen, D. Lee, A.R. Yan, Chin. Phys. B 23 (2014) 107501.
[16] C.J. Yan, S. Guo, R.J. Chen, D. Lee, A.R. Yan, IEEE Trans. Magn. 50 (2014) 2102605.
[17] Z.B. Li, M. Zhang, B.G. Shen, J.R. Sun, Appl. Phys. Lett. 102 (2013) 102405.
[18] Z.B. Li, B.G. Shen, M. Zhang, Y. Zhang, F.X. Hu, J.R. Sun, Appl. Phys. Lett. 106 (2015) 042403.